Research Square

Preprints are preliminary reports that have not undergone peer review.
They should not be considered conclusive, used to inform clinical practice,
or referenced by the media as validated information.

Synergistic Fire Protection and Water Resistance of Intumescent Coatings via Surface- Engineered Shell-Derived Biogenic Inorganic Particles

Wenzhou Du
Shandong University of Science and Technology
Guizhuang Zhu
Shandong University of Science and Technology
Luyao Wang
198637078800163.com

Shandong University of Science and Technology
Mingxue Huang
Shandong University of Science and Technology
Yangxu Wang

Research Article

Keywords: Shell-derived biogenic inorganic particles, Intumescent fireproof coating, Interfacial engineering, Synergistic flame retardancy, Water resistance

Posted Date: October 30th, 2026

DOI: https://doi.org/10.21203/rs.3.rs-11192829/v1

License: This work is licensed under a Creative Commons Attribution 4.0 International License.
Read Full License

Additional Declarations: No competing interests reported.

Synergistic Fire Protection and Water Resistance of Intumescent Coatings via Surface-Engineered Shell-Derived Biogenic Inorganic Particles

Abstract

Steel-structure intumescent fire-retardant coatings suffer from poor water resistance and weak high-temperature char layers. Herein, shell-derived biogenic inorganic particles (SBIPs) were surface-functionalized with KH-550 and incorporated as a bio-based synergistic filler into silicone-acrylic/epoxy waterborne intumescent coatings (IFR-EP/SAE). Characterizations including combustion simulation, thermogravimetry, limiting oxygen index (LOI), cone calorimetry, SEM, and Raman spectroscopy were performed to investigate interfacial compatibility, fire protection, thermal stability, water-aging resistance, and char evolution. KH-550 functionalization improved SBIP–matrix compatibility, while a distinct biphasic concentration-dependent effect on flame retardancy was observed, with 3 wt.% SE-SBIPs showing optimal performance. Compared with the blank control, the addition amount of 3 wt. % reduced the peak back-side steel temperature to 289.27 °C, increased the LOI to 42.5%, and raised the initial rapid thermal-degradation temperature from 304 to 363 °C. After 48 h water immersion, it maintained favorable flame-retardant and smoke-suppression performance, with reduced peak heat-release rate and total smoke release. Raman analysis showed a decreased ID/IG ratio from 1.36 to 1.07, indicating enhanced char graphitization. This work provides a sustainable strategy for developing durable bio-based fire-protective coatings.

Keywords: Shell-derived biogenic inorganic particles; Intumescent fireproof coating; Interfacial engineering; Synergistic flame retardancy; Water resistance.

1 Introduction

In recent years, coal mine fires have become the main bottleneck restricting the development of coal resources.[1-3]. Most of the various types of underground infrastructure are based on steel structures. Common components include belt roadway load-bearing steel frames, roadway support supports, chamber steel structural components, and ventilation air doors. When the fire temperature of steel structure reaches 600 ℃ or higher, the mechanical strength decreases rapidly and the main bearing capacity is lost.[4, 5]. The intumescent fire retardant coating can generate a dense intumescent carbon layer by heating, which can effectively block the heat conduction between the fire source and the matrix. It is a common fire protection method for steel structures.[6-10]. Intumescent fire retardant coating is composed of acid source, carbon source, gas source, flame retardant filler and polymer binder[11-16]. Filler plays a key role in intumescent fire retardant coatings, which is used to improve the water resistance and fire resistance of the coatings. At the same time, the filler can also act as a carbon source to participate in the carbon formation reaction of the coatings, improve the quality of the carbon layer and enhance the flame retardancy of the carbon layer.[17-21].

At present, the fillers of intumescent fire retardant coatings can be divided into inorganic fillers and biological fillers. The common inorganic fillers are TiO_2, SiO_2, $Al(OH)_3$, $Mg(OH)_2$, $CaCO_3$ and ZnO. CHAISAENRITH et al.[22] isotactic acrylic-based intumescent fire retardant coatings doped with nano-TiO_2. The experimental results show that the modified intumescent carbon layer is continuous and dense, the porosity is increased, the structure is not easy to peel off, and the thermal insulation and barrier effect is excellent. Zhang et al.[23] prepared α-ZrP @ MnHP layered nanofillers to prepare organic-inorganic halogen-free flame-retardant coatings. The characterization results showed that the components were uniformly dispersed and the interface reaction occurred. Some scholars have found that TiO_2 as a filler

can significantly improve the stability of the carbon layer, which can effectively improve the thermal insulation performance of the carbon layer.[18]. Shi et al.[24] synthesized the water-soluble cage-type flame-retardant PAPEG, whose gradient thermal decomposition enhances charring capacity. Transparent intumescent fireproof coatings were prepared by compounding PAPEG with trioxymethylene. At the optimal formulation ratio, a dense and heat-insulating carbon layer can be formed, which significantly extends the fire resistance time of wood panels. Wang et al.[25] adopted the compound of graphene and carbon nanotubes as flame-retardant filler for waterborne intumescent coatings and verified the flame-retardant synergistic effect between them. When the mass ratio of graphene to carbon nanotubes was 3:1, the coating presented the best thermal insulation, charring and flame-retardant indices, while the single addition of graphene resulted in better water resistance and mechanical properties. Yan et al.[26] introduced nanosilica into cyclic phosphate flame-retardant via chemical grafting to fabricate high transparent intumescent fireproof coatings. A synergistic effect exists between phosphorus and silicon. An appropriate amount of nanosilica can enhance the thermal stability of the coating, form a dense expandable carbon layer, and simultaneously achieve remarkable smoke suppression and reduce heat release.

Biological fillers, such as biomass ash and biologically fibers, have gained increasing applications in recent years due to their environmental friendliness, nature as renewable biological resources and cost-effectiveness[27, 28]. In the field of fire retardant coatings, the first application is mainly high calcium content biological fillers, such as egg shells and shells with calcium carbonate as the main component. Due to its rich natural hydroxyl and aromatic groups, excellent thermal expansion performance and thermal stability, it can be used as a bio-based filler with excellent performance[29, 30]. WANG et al.[31] prepared clam shell CMS, conch shell CHS and egg shell CES three kinds of biological fillers. Through

cone calorimetry, large plate fire resistance, smoke density, TG, SEM characterization and comparison tests, the optimal ratio was obtained and the mechanism of carbon layer crosslinking, smoke suppression and heat insulation was revealed[32]. Biological fillers such as eggshell calcium carbonate can be used to prepare intumescent flame retardant coatings. Shell powder can adjust the enthalpy of flame retardant coatings, increase the amount of carbon formation, and do not damage the light transmittance[33]. Yew et al.[34] prepared acrylic intumescent flame-retardant coatings by using waste eggshell as an environmentally friendly biological filler. Studies have shown that egg shell-based inorganic composite fillers can promote a dense heat-insulating carbon layer and improve the heat resistance, water resistance and adhesion properties of the coating. BEH et al.[35] conducted microscopic analysis on burnt rubber wood biomass ash and found that it contains abundant O−H, P−O−C and P−O functional groups, all of which can improve the compactness of the carbon layer and its heat barrier effect. Nasir et al.[36] investigated the synergistic carbon formation mechanism of biological fillers and inorganic fillers. Rice husk ash (RHA), chicken eggshell (CES), TiO_2 and $Al(OH)_3$ were added in different ratios into the (APPII)/PER/MEL intumescent flame-retardant system. The experimental results indicated that the coating with 5 wt.% TiO_2 and 5 wt.% RHA achieved the best fireproof performance in the simulated combustion test, showing a 19% improvement compared with the coating without biological fillers. After 48 h of water immersion test, the coating added with RHA exhibited favorable water resistance, while the coating added with CES performed poorly but was still superior to the fireproof coatings only added with inorganic fillers TiO_2 and $Al(OH)_3$. The experiment also demonstrated that the coating presented the worst water resistance when RHA, CES, TiO_2 and $Al(OH)_3$ were added simultaneously.

Under the current social background of emphasizing green environmental protection and energy conservation and emission reduction, intumescent fire retardant coating has been widely concerned and

valued in the fire prevention work of mine steel structure due to its characteristics of less materials, convenient construction and low cost. However, the quality of commercially available intumescent fireproof coatings for steel structures varies widely, with common deficiencies including inferior flame-retardant property, low carbon layer strength and poor water resistance. In addition, with the increasingly stringent safety requirements for mine steel structures, existing intumescent fireproof coatings can no longer satisfy the current market demands. Although the traditional intumescent flame-retardant system APP-MEL-PER delivers excellent fire retardant performance, it exhibits unsatisfactory water resistance. Accordingly, it is of great importance to explore appropriate materials to improve traditional intumescent fireproof coatings.

In this study, MPP, PET / DPER and MEL were used as acid source, carbon source and gas source respectively, and the matrix resin mixed with silicone-acrylic emulsion and epoxy emulsion was used as the matrix of intumescent fire retardant coating. Shell-derived biogenic inorganic particles (SBIPs) and TiO_2 were selected as biological filler and inorganic filler respectively. To overcome the inherent interfacial defects and enhance the compatibility of the SBIPs with the hybrid emulsion, surface functionalization was executed using the silane coupling agent KH-550. The synergistic effects of varying loadings of SE-SBIPs and TiO_2 on the flame retardancy, char-forming robustness, and water resistance of the intumescent coatings were systematically investigated through simulated large-panel combustion, LOI, cone calorimetry, and structural analyses.

2. Experimental Methods and Materials

2.1 Experimental Materials

Melamine polyphosphate (MPP, purity: 99%) was purchased from Suqian Zhenxing Chemical Co., Ltd. Melamine (MEL, purity: 99%), polyethylene terephthalate (PET, form: granular), dipentaerythritol

(DPER, purity: 90%), titanium dioxide (TiO_2, purity: 99.8%, rutile), and silane coupling agent (KH-500, purity: 99%) were purchased from Shanghai Macklin Biochemical Co., Ltd. Waterborne epoxy resin (solid content: 55%) was purchased from Zhengzhou Xingwang Chemical Co., Ltd. silicone-acrylic emulsion (solid content: 50%) was purchased from Henan Dazao Chemical Products Co., Ltd. The raw biogenic precursor (shell-derived, 200 mesh) was self-prepared in the laboratory.

2.2 Preparation of Experimental Samples

2.2.1 Preparation and Characterization of SBIPs

SBIPs has been verified to have great potential as a bio-based flame retardant filler due to its unique laminar structure and good thermal stability, showing excellent smoke suppression and anti-aging properties. However, due to the compatibility problem between SBIPs and organic matter, agglomeration is easy to occur, resulting in a decrease in flame retardant effect. Therefore, it is necessary to modify it to improve its compatibility with the surface of organic matter.[37]. First, surface impurities were removed. The shells were immersed in 0.05 mol/L HCl solution for 3 h, and then soaked in 0.20 mol/L NaOH solution for 3 h. After soaking, the shells were taken out and rinsed with deionized water to eliminate surface contaminants, and then naturally dried at room temperature to obtain clean shells. Subsequently, the shells were ground. The dried, clean shells were pulverized in a grinder, and SBIPs was obtained after passing through a 200-mesh sieve. Meanwhile, the composition of SBIPs was characterized by X-ray diffractometer (XRD), Fourier transform infrared spectroscopy (FTIR) and X-ray fluorescence spectrometry (XRF). The preparation process of SBIPs and the characterization results are presented in Figure 1(a) and Table 1, respectively.

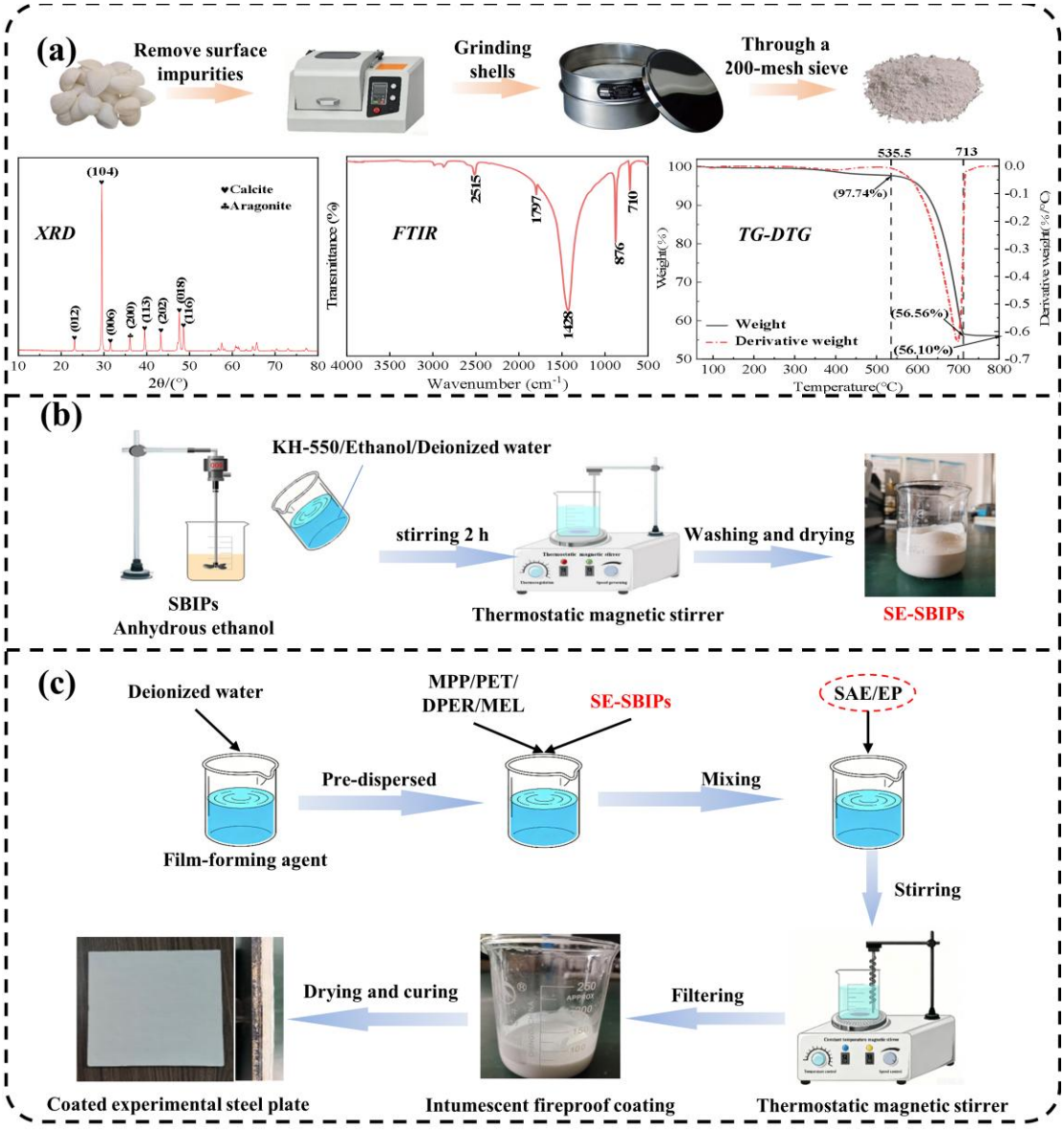


Fig.1. The flowchart of preparation

Table 1 The table of oxide composition of calcined SBIPs obtained by XRF

Oxide composition	CaO	Na_2O	Fe_2O_3	SiO_2	MgO	Al_2O_3	SrO	K_2O	P_2O_5
wt.%	97.135	0.684	0.222	0.604	0.098	0.426	0.402	0.051	0.055

As shown in Figure 1(a), comparative analysis of the SBIPs XRD pattern and the standard XRD pattern of calcium carbonate (NO.54-1272) reveals that SBIPs is mainly composed of $CaCO_3$, which is dominated by the calcite-type $CaCO_3$ with excellent mechanical properties, and contains a small amount

of aragonite-type $CaCO_3$. The FTIR spectrum of SBIPs shows a narrow and weak in-plane bending vibration peak of CO_3^{2-} at 710 cm^{-1}, a narrow and intense CO_3^{2-} out-of-plane bending vibration peak at 876 cm^{-1}, and a broad and strong CO_3^{2-} antisymmetric stretching vibration peak at 1428 cm^{-1}, verifying the presence of calcium carbonate. Meanwhile, absorption peaks associated with C−H and −OH groups are detected, indicating a small amount of organic matter in SBIPs. As presented in Table 2, XRF results of the SBIPs residue calcined at 800 ℃ show that the calcined sample consists primarily of 97.135 wt.% CaO, along with trace oxides including Na_2O, SiO_2, and Fe_2O_3, further confirming calcium carbonate as the main component of SBIPs.

According to the thermogravimetric curve of SBIPs, its mass loss is divided into three stages: 60 ℃–535.5 ℃, 535.5 ℃–713 ℃, and 713 ℃–800 ℃. The mass loss in the range of 60 ℃–535.5 ℃ reaches 2.26%, with a slow mass loss rate and no prominent derivative thermogravimetric (DTG) peak. This is attributed to the volatilization of adsorbed water and bound water as well as the decomposition of organic matter such as proteins and polysaccharides, indicating a low organic content in SBIPs. In the second stage, the mass loss rate increases sharply, with the mass decreasing from 97.74% to 56.56% and a intense DTG peak appearing, which corresponds to the high-temperature decomposition of calcium carbonate into CaO and CO_2. In the range of 713 ℃–800 ℃, the mass loss is merely 0.46% with a flat mass loss curve, suggesting that the decomposition of calcium carbonate is essentially completed, and that the residual mass at 800 ℃ is 56.10%. In summary, the total content of water and organic matter in SBIPs is 2.26%, and the decomposition of calcium carbonate essentially terminates at 713 ℃, demonstrating excellent thermal stability.

2.2.2 Surface Functionalization of SBIPs

Owing to the poor compatibility between SBIPs and the polymer matrix, SBIPs exhibits

unsatisfactory dispersion in emulsions and is prone to agglomeration. Surface functionalization of SBIPs was performed using the silane coupling agent KH-550. First, 50 g of SBIPs was weighed, mixed with an appropriate amount of anhydrous ethanol, and stirred until homogeneous to prepare a SBIPs slurry. Then, 5 mL of hydrolyzed silane coupling agent solution was prepared at a volume ratio of KH-550 to ethanol to deionized water of 20:72:8, and stirred for 20 min to ensure sufficient hydrolysis of the silane coupling agent. Finally, the hydrolyzed silane coupling agent solution was slowly added dropwise to the SBIPs slurry. After being stirred for 2 h in a water bath at 75 ℃ to allow complete reaction, the product was washed sequentially with anhydrous ethanol followed by deionized water, and dried in an oven to obtain surface-engineered SBIPs (SE-SBIPs). The functionalization process of SBIPs is shown in Figure 1(b), and the four-step reaction mechanism of SBIPs modified by silane coupling agent is illustrated in Figure 2.

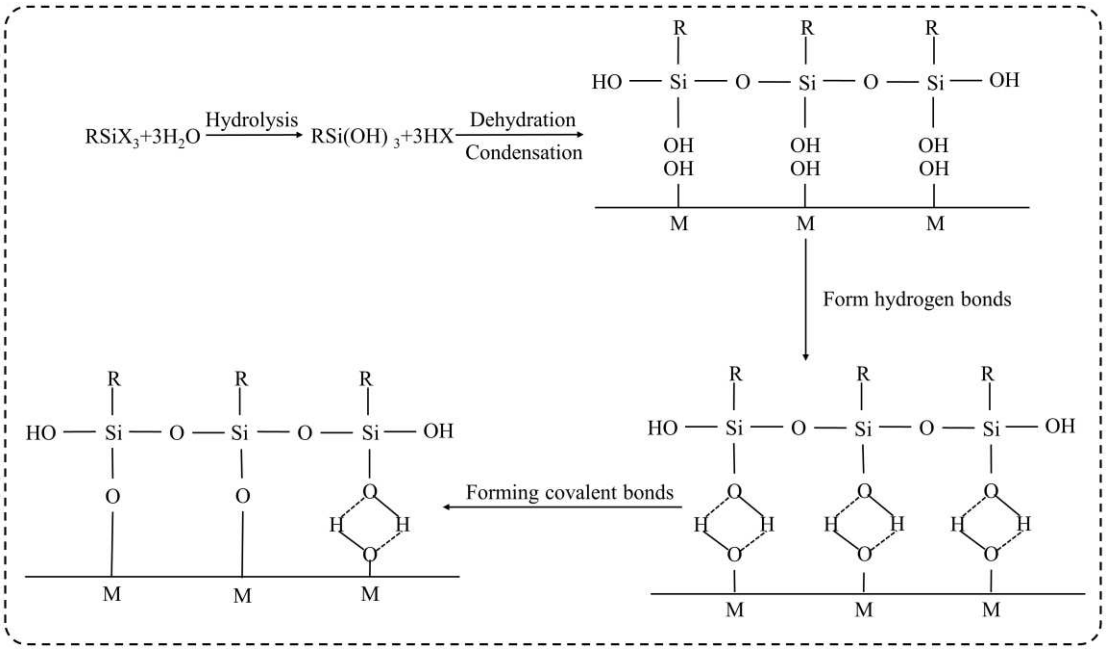


Fig.2. Theoretical model of the four-step reaction of silane coupling agents

First, the X groups in the silane coupling agent R−Si−X_3 undergo hydrolysis to form the silanol R−Si−$(OH)_3$, followed by dehydration condensation between Si−OH groups to generate silane oligomers

containing Si−OH groups. Subsequently, the Si−OH groups in the silane oligomers form hydrogen bonds with the −OH groups on the surface of the SBIPs. During the heat curing process, the hydroxyl groups linked by these hydrogen bonds undergo dehydration and form Si−O−M covalent bonds with the SBIPs. The surface modification effect of SBIPs was verified via scanning electron microscopy (SEM) characterization on SBIPs before and after modification, as well as by observing and comparing their micromorphology and dispersion states in the mixed emulsion.

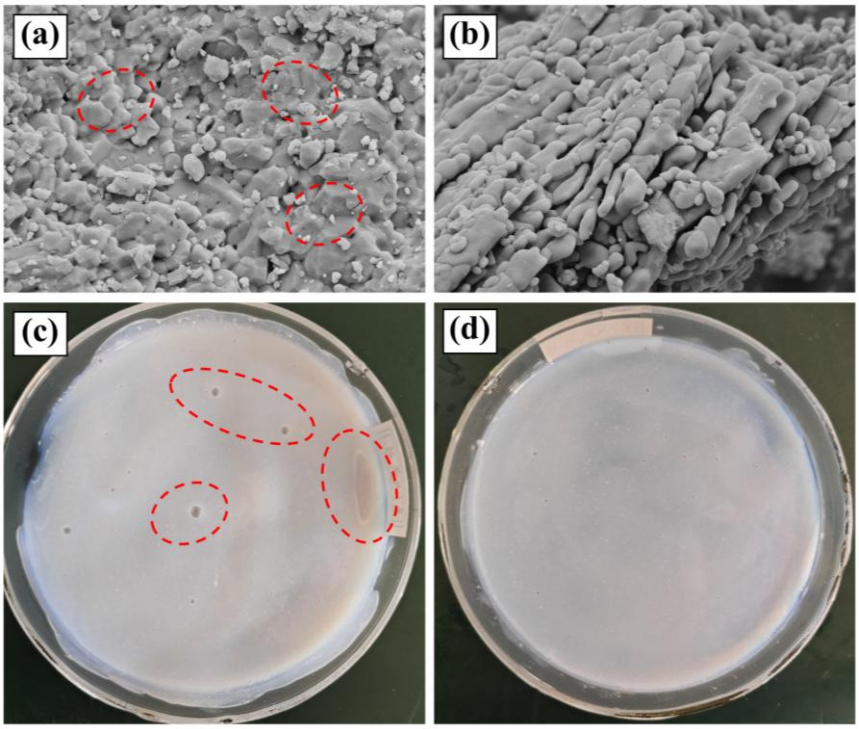


Fig.3. Analysis of the effects of surface functionalization on SBIPs

Figures 3(a) and 3(b) present the scanning electron microscopy images of SBIPs and SE-SBIPs. Comparison reveals that SBIPs have indistinct boundaries and exhibit obvious interparticle adhesion, and the particles vary in size and morphology, mostly in irregular shapes. In contrast, SE-SBIPs feature rounder surfaces, clearer interparticle boundaries, and more uniform particle size distribution. Figures 3(c) and 3(d) display the dispersion states of SBIPs and SE-SBIPs samples in the mixed emulsion. As can be clearly seen from Figure 3(c), there are prominent white granular agglomerates in the mixed

emulsion, indicating that SBIPs can not be uniformly dispersed in the emulsion and exhibits severe agglomeration. Direct incorporation of SBIPs as a filler may adversely affect its physicochemical and flame-retardant properties. Figure 3(d) shows the dispersion state of SE-SBIPs in the emulsion. Comparative analysis reveals that SE-SBIPs exhibits uniform dispersion in the emulsion, with it uniformly distributed and no obvious agglomeration detected.

The above results demonstrate that the surface modification of SBIPs with the silane coupling agent KH-550 effectively reduces the tendency of SBIPs to agglomerate in the emulsions. SE-SBIPs disperses uniformly in the emulsion, this uniform dispersion also facilitates its dispersion as a filler in the coating system.

2.2.3 Preparation of Intumescent Flame Retardant Coating

In previous studies, the optimal ratio of the intumescent flame-retardant system in IFR-EP/SAE was experimentally determined to be a mass ratio of MPP to PET DPER to MEL of 22:1:8:1. The matrix resin constitutes 47 wt.% of the coating, of which the epoxy emulsion and silicone-acrylic emulsion account for 32.9 wt.% and 14.1 wt.% of the total coating mass respectively[38]. Building on previous work, this study examines the filler loading in the coatings and analyzes the effect of SE-SBIPs loading on the flame-retardant properties and water resistance of the coating. A total of five groups of coating formulations with different filler ratios were designed, designated SP1–SP5, as presented in Table 2.

Table 2 The formulations of intumescent fire-retardant coatings with different filler ratios

Sample	Composition percentages/ wt.%				
	SP1	SP2	SP3	SP4	SP5
Epoxy emulsion/ silicone-acrylic emulsion	32.9/14.1	32.9/14.1	32.9/14.1	32.9/14.1	32.9/14.1
MMP/PET/DPER/MEL	22/1/8/1	22/1/8/1	22/1/8/1	22/1/8/1	22/1/8/1
TiO_2	1	1	1	1	1
SE-SBIPs	0	1	2	3	5
Film-forming additive	1	1	1	1	1
Deionized water	19	18	17	16	14

First, a small quantity of coating additives was added into a beaker, and an appropriate amount of deionized water was then added for pre-dispersion. Subsequently, the optimally proportioned MPP-PET-DPER-MEL intumescent flame-retardant system was added to the beaker together with SE-SBIPs used in this work, and the mixture was thoroughly mixed for 30 min at a stirring speed of 800 r/min using a high-speed stirrer. Next, the binders (EP-SAE) were added to the well-mixed slurry, followed by further mixing for 90 min at a stirring speed of 400 r/min. After homogeneous mixing, the slurry was filtered through a 200-mesh sieve to obtain the intumescent fireproof coating. The as-prepared coating was brushed-coated onto a 100 mm × 100 mm × 2 mm steel plate, with a thickness of approximately 1.5 mm. The preparation process of the intumescent fireproof coating is shown in Figure 1(c).

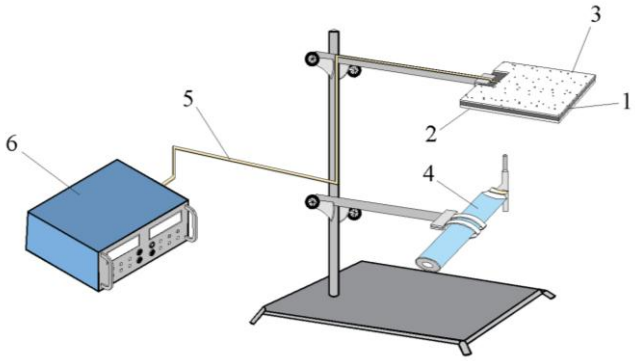
2.3 Testing and Characterization

2.3.1 Thermogravimetry Experiment

In this study, thermogravimetric analysis of SBIPs was performed using a TA Q600 simultaneous thermal analyzer. The measurement was conducted in an N_2 atmosphere at a heating rate of 10 ℃/min over a temperature range of 30 ℃–800 ℃, to investigate the thermal stability of SBIPs as a filler in intumescent fireproof coatings.

2.3.2 The large-panel combustion simulation experiment

The intumescent fireproof coating was uniformly brush-coated onto a 100 mm × 100 mm × 2 mm Q235B steel plate. The coated sample was dried naturally at room temperature, and 12-15 coating cycles were applied to achieve a dry film thickness of 1.5 mm ± 0.1 mm, followed by curing at room temperature for 7 d. A vertical combustion test device was constructed in accordance with the vertical combustion principle. A butane gas torch was fixed vertically on an iron stand, and the steel plate sample was mounted on the stand with the center of the coating directly facing the spray gun at a distance of 80 mm. Heat-insulating cotton was laid on the back of the steel plate to eliminate interference from ambient temperature. A K-type thermocouple connected to a digital thermometer was attached to the center of the back surface to collect real-time back temperature data, and the peak temperature (Tmax) was recorded. The device is shown in Figure 4.



1：Steel plate；2：Coating；3：Heat-insulating cotton；4：Butane gas torch；5：K-type thermocouple；6：Digital thermometer。

Fig.4. The fire test device

2.3.3 Limiting Oxygen Index Test

In this study, limiting oxygen index tests were conducted on the coatings using an intelligent integrated oxygen index tester equipped with a fume hood manufactured by TESTech. For each coating group, five rectangular samples with dimensions of 100 mm × 10 mm × 3 mm were prepared. The test was performed under a mixed atmosphere of oxygen and nitrogen, with a flow control accuracy of ±0.2%. The vertically mounted samples were ignited at the top with a flame, with an ignition duration of ≤ 30 s. The minimum oxygen concentration at which the sample exhibits a burning length of ≤ 40 mm was recorded.

2.3.4 Cone calorimetry test

In this study, cone calorimetry tests were performed on the coating samples using a Tech-GBT16172 cone calorimeter. Sample preparation and testing procedures were performed in accordance with the ISO 5660-1 standard. Each sample had dimensions of 100 mm × 100 mm × 3 mm. The test was conducted at a radiant heat flux of 50 kW/m^2 with a working distance of 25 mm. The mass of each sample was approximately 40 g. During testing, the unexposed surface of the sample was wrapped in aluminum foil to prevent molten droplets from contaminating the instrument and interfering with mass loss rate

measurements.

2.3.5 Scanning Electron Microscopy (SEM) Analysis

In this study, a ZEISS-SIGMA HD scanning electron microscope was employed to observe the micromorphology of the carbon layer formed after the cone calorimetry test on water-immersed coating samples, at magnifications ranging from 30 times to 5000 times. During SEM observation, the accelerating voltage was set to15 kV and the working distance was 8 mm.

2.3.6 Raman Spectroscopy Analysis

In this study, a DXR Raman Microscope manufactured by Thermo was employed to characterize the carbon layer formed after combustion of the coating. The D and G peak values of the Raman spectrum were obtained via peak fitting, which were used to analyze the strength of the carbon layer. The test was performed at an excitation wavelength of 532 nm and a measurement range of 800 cm^{-1} to 2000 cm^{-1}.

3. Results and Discussion

3.1 Analysis of the Large-panel Combustion Simulation Experiment for Coatings

Figures 5(a) and 5(b) present the macroscopic morphologies of five groups of coating samples (SP1–SP5) before and after combustion, respectively. As can be observed from Figure 5(a), all five coating groups exhibit good film-forming properties with smooth surfaces, and no cracks or surface irregularities are detected, indicating that the addition of SE-SBIPs exerts no adverse effect on the film-forming property of the coatings. In addition, with the increase in SE-SBIPs content, the coating surface exhibits slight yellowing, a phenomenon that may be attributed to the slightly yellowish-white hue of SE-SBIPs and impairs the decorative properties of the coatings to a certain extent. As shown in Figure 5(b), the carbon layer of SP1 (with no SE-SBIPs) exhibits multiple prominent cracks and collapsed structures. These cracks act as heat transfer pathways between the substrate and the fire source,

weakening the thermal insulation effect of the carbon layer. With increasing SE-SBIPs content, the cracks on the carbon layer surface of each sample gradually decrease. A small number of cracks emerge at the center of the carbon layer of sample SP2. The carbon layer of SP3 is relatively intact, yet a large quantity of white particulate matter appears on its surface. These particles are residues formed by oxidation and dehydration of the carbon layer at high temperatures, indicating the poor fire resistance of the SP3 carbon layer. No obvious cracks are observed on the carbon layer surface of SP5, but the expansion property of its carbon layer is unsatisfactory. This phenomenon indicates that excessive SE-SBIPs inhibits the expansion ratio and charring performance of the carbon layer. Excessive SBIPs (main component $CaCO_3$) decomposes into CaO at high temperature, which can react with phosphoric-acid-containing fragments thermally decomposed from MPP acid source to form thermally stable calcium phosphate ($Ca_3(PO_4)_2$). This acid-base solid-state reaction consumes considerable active phosphorus species that are originally responsible for catalyzing esterification and char-forming reactions between the acid source and carbon source. Consequently, insufficient active phosphate components remain in the intumescent system, restraining the expansion and char-building process, and ultimately deteriorating the fire-insulating performance at higher SBIPs loading. The carbon layer of SP4 doped with 3 wt.% SE-SBIPs features a dense structure free of obvious cracks and collapsed structures. These results further confirm that an appropriate amount of SE-SBIPs is critical for endowing the coating with excellent charring and thermal insulation properties.

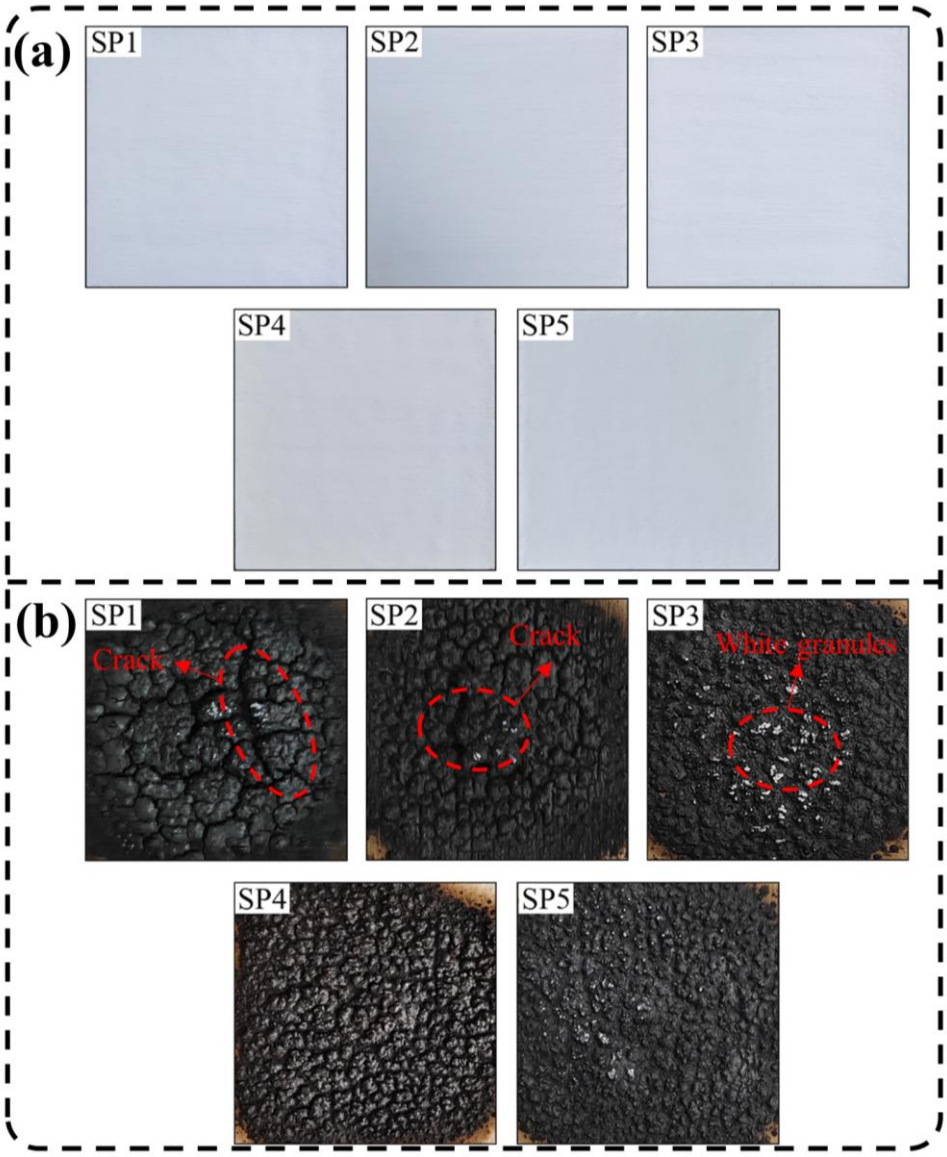


Fig.5. The morphologies of SP1–SP5 coated samples before and after combustion

Figure 6 (a) presents the back temperature curves of the steel plate coated with coatings SP1–SP5 during the large-panel combustion simulation experiment. As shown in the figure, the back temperatures of the steel plates for all five coating groups rose rapidly within 5 minutes after the initiation of the experiment, indicating that the heat barrier effect of the coatings in this initial stage mainly derived from their inherent physical properties. Between 5 and 15 minutes of the experiment, the back temperature of the steel plate with sample SP4 remained consistently low, whereas that of sample SP5 increased sharply from 171.3 ℃ to 309.4 ℃. This phenomenon may be caused by the negative effect of excessive SE-

SBIPs on the expansion and charring reaction of the coating, which is consistent with the poor expansion performance of the SP5 carbon layer shown in Figure 5. After 20 minutes, all samples essentially reached their respective equilibrium back temperatures. Among these samples, sample SP4 exhibited the lowest equilibrium temperature of 288.3 ℃, while sample SP5 showed the highest equilibrium temperature of 339.5 ℃. Figure 6 (b) presents the peak back temperature of steel plate (Tmax) for coatings SP1–SP5 during the large-panel combustion simulation experiment. The highest Tmax of 341.17 ℃ is observed for coating SP5, while coating SP4 achieves a Tmax of 289.27 ℃ and shows the best flame-retardant properties. This phenomenon can be explained by the fact that an appropriate amount of filler enables sufficient expansion of the coating and the formation of an intact carbon layer.

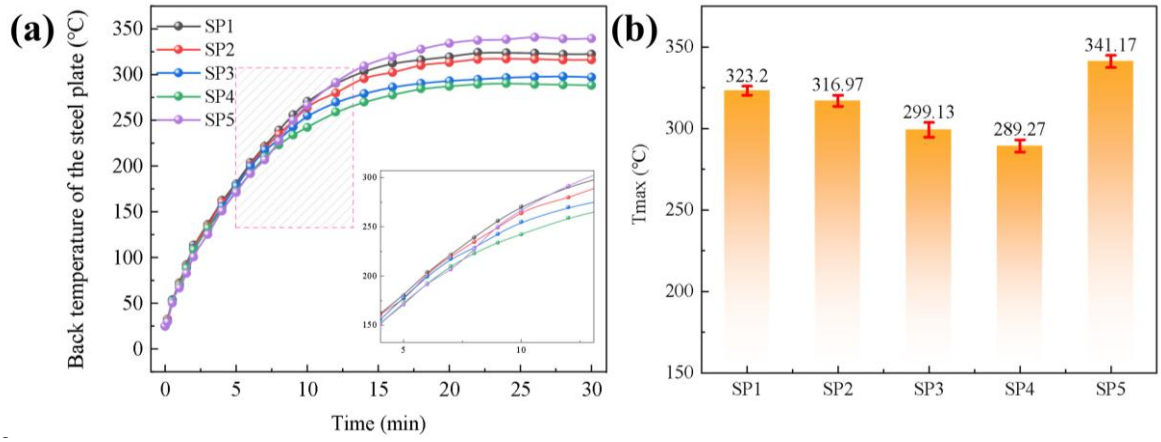


Fig.6. (a)Back temperature curve of SP1-SP5 steel plate and (b) Peak back temperature (Tmax) of P1-SP5 coated steel sheet

Overall, the back temperature of the steel plate for the samples decreased significantly with the addition of an appropriate amount of SE-SBIPs. At the 30th minute of the experiment, the back temperatures of the steel plate for samples SP2 to SP5 were 316.2 ℃, 297.1 ℃, 288.3 ℃ and 339.5 ℃, respectively. It can be observed that when the content of SE-SBIPs reached 5 wt.%, the back temperature of the steel plate rose, indicating a decline in thermal insulation performance. This phenomenon is attributed to the adverse effect of excessive SE-SBIPs on the expansion performance of the carbon layer.

Notably, sample SP4 doped with 3 wt.% SE-SBIPs exhibited the optimal thermal insulation performance. Based on the above results, it can be concluded that the addition of an appropriate amount of SE-SBIPs can effectively improve the flame-retardant property of IFR-EP/SAE.

3.2 Analysis of the Thermal Stability of Coatings

Figures 7(a) and 7(b) present the TG and DTG curves of coatings SP1 and SP4. As revealed by the TG and DTG test results, compared with SP1 (without SE-SBIPs), SP4 doped with SE-SBIPs exhibits significantly improved thermal stability and flame-retardant properties. SP1 enters the rapid thermal degradation stage at approximately 304 ℃, with its maximum mass loss rate occurring at 379 ℃, while SP4 enters the same stage at around 363 ℃ and its peak mass loss rate appears at 484 ℃. At low temperatures, SP1 undergoes more intense decomposition reactions and exhibits a higher mass loss rate than SP4. In contrast, both the initial rapid decomposition temperature and the temperature corresponding to the maximum mass loss rate of SP4 shift significantly toward higher temperatures; the maximum thermal decomposition temperature rises to above 400 ℃, and the main degradation interval shifts to higher temperatures as a whole. This indicates that SE-SBIPs effectively inhibits the early thermal decomposition of the matrix and delays the release of combustible degradation products. Within the critical combustion temperature range of 300 ℃–600 ℃, the residual mass of SP4 is consistently higher than that of SP1, indicating a synergistic charring effect between SE-SBIPs and the intumescent flame-retardant system. This effect promotes the early formation of a dense and stable carbon layer, and restricts heat transfer and the escape of combustible gases via the barrier effect of the condensed phase. Although the two groups of samples exhibit similar final char yield at 800 ℃, the superior thermal stability and protective effect of the carbon layer of SP4 in the low-to-medium temperature range endow it with better flame-retardant properties.

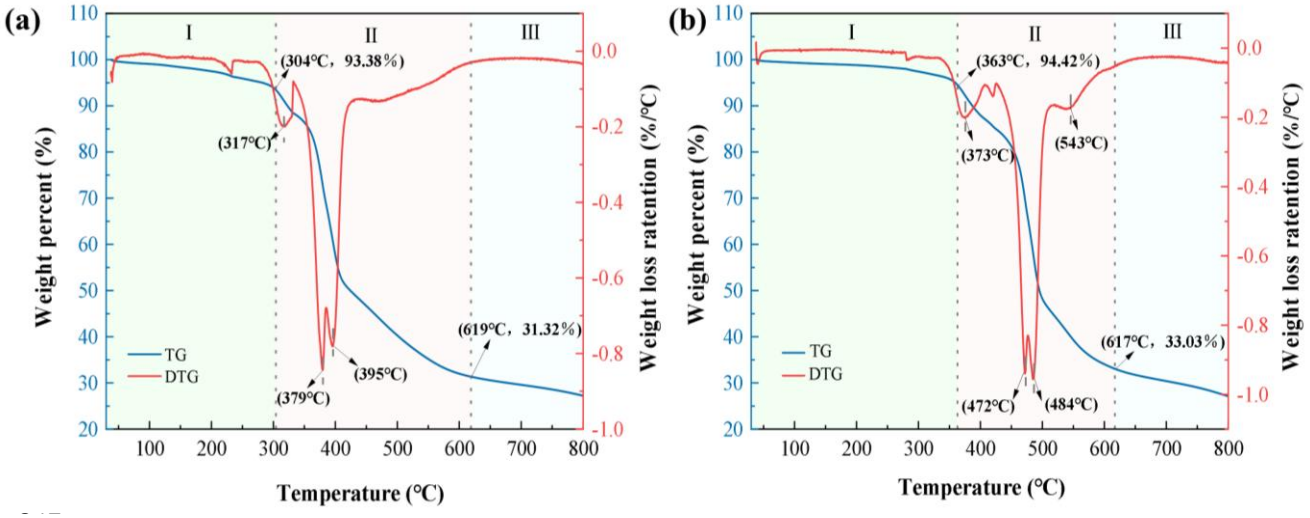


Fig.7. The TG (a) and DTG (b) curves of SP1 and SP4 coated samples

3.3 Analysis of the Limiting Oxygen Index

The large-panel combustion simulation experiment was carried out in the aforementioned study to investigate the flame-retardant properties of coatings SP1 to SP5, and coating SP4 was found to exhibit the optimal flame-retardant performance. In this test, the limiting oxygen index (LOI) test, a more intuitive characterization method, was employed to analyze the flame-retardant properties of coating SP1 (without SE-SBIPs) and coating SP4 doped with 3 wt.% SE-SBIPs.

Figure 8 presents the combustion behavior and test results of coating samples SP1 and SP4 after the limiting oxygen index test. The results indicate that the oxygen indices of coating samples SP1 and SP4 were 40.5% and 42.5%, respectively. Both samples self-extinguished when removed from the flame at these oxygen concentrations, with a combustion duration of less than 180 s for each. Both coatings exhibited excellent flame-retardant properties, meeting the flame-retardant criteria. The oxygen index of coating SP4 was 2 percentage points higher than that of coating SP1, indicating that SP4 had a lower tendency to sustain combustion at the same oxygen concentration and exhibited better flame-retardant performance. This demonstrates that coating SP4 forms a denser carbon layer structure after combustion, with lower heat release and higher resistance to oxygen diffusion during the combustion process. The

limiting oxygen index test results confirm that the synergistic flame-retardant effect of SE-SBIPs has a promoting effect on the overall flame-retardant properties of the coating and effectively improves its flame-retardant performance. At the same oxygen concentration, the coating doped with SE-SBIPs is less likely to sustain continuous combustion.

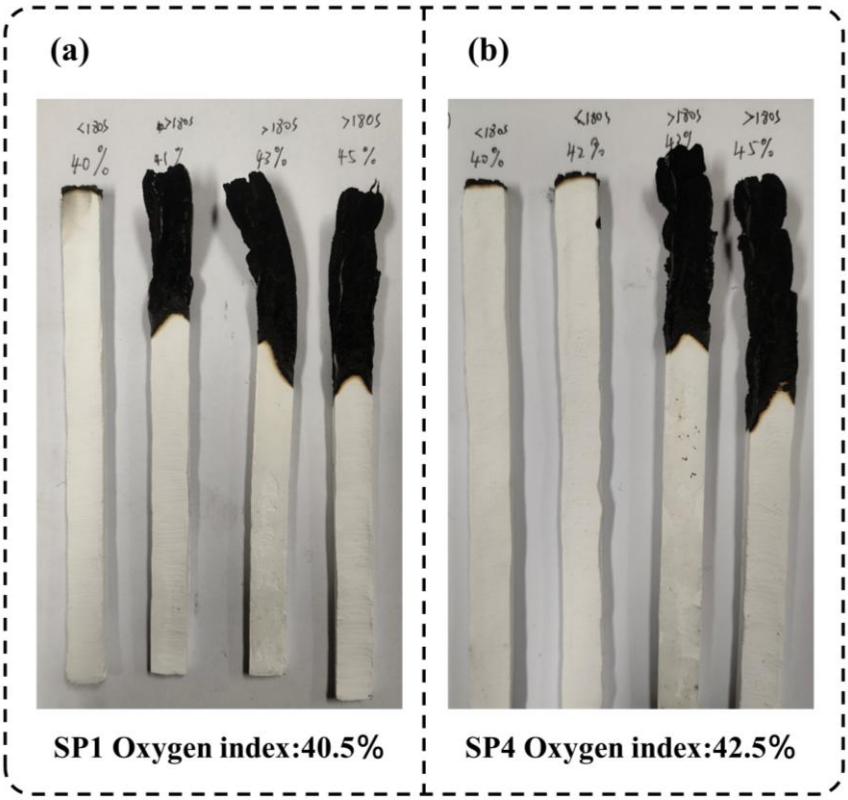


Fig.8. Limiting oxygen index test results of SP1 and SP4 coated samples

3.4 Analysis of the Large-panel Combustion Simulation Experiment for Coatings Before and After Water Immersion

Water resistance tests were conducted to investigate the effect of SE-SBIPs on the water resistance of coatings. Coatings SP1 and SP4 were subjected to 48 h of water immersion followed by drying, and were denoted as SP1-48h and SP4-48h, respectively. The large-panel combustion simulation experiment was performed on coatings SP1 and SP4 both before and after 48 h of water immersion.

Figure 9 illustrates the temperature-time curves of the back-side temperature of the steel plate for

the coatings. In the large-panel combustion simulation experiment, the back-side temperature curves of the steel plate for the two intumescent fire-retardant coatings SP1 and SP4 showed a consistent trend both in the pristine state and after 48 h of water-immersion aging. All samples underwent a rapid temperature rise within 0 to15 min in the initial combustion stage. As the coating expanded under heating to form a carbonaceous thermal insulation layer, the temperature rise rate gradually slowed and eventually leveled off. After 48 h of water immersion, the back temperatures of SP1-48h and SP4-48h were both higher than those of their corresponding pristine samples. This was attributed to the fact that water immersion caused water absorption and degradation of the coating resin matrix, leaching loss of small-molecule flame-retardant components, and reduction in the interfacial bonding strength of the coating, leading to a loose and porous char structure, a sharp decline in thermal insulation performance, and overall deterioration of fire-retardant performance. Throughout the post-immersion test, the temperature rise of SP4-48h remained lower than that of SP1-48h, with a significantly lower steady-state temperature. This demonstrates that the addition of SE-SBIPs improves the water resistance of the coating. It mitigates the performance degradation induced by water immersion through cross-linking the matrix, anchoring active flame-retardant substances and reinforcing the carbon layer framework of the carbon layer, thus endowing the coating with superior water resistance, durability and fire resistance.

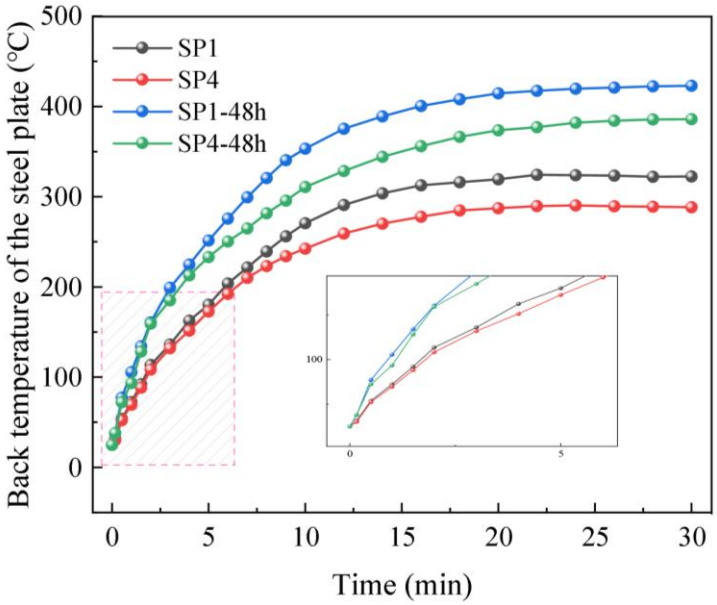


Fig.9. The back temperature curve of the steel plate after 48h of immersion in water in the large-panel combustion simulation experiment

3.5 Analysis of Cone Calorimetry Testing of Coatings After Water Immersion

To investigate the effect of SE-SBIPs on the water resistance of coatings, coatings SP1 and SP4 were first subjected to 48 h of water immersion, followed by cone calorimetry tests after drying. Table 3 perents the time to ignition (TTI), peak heat release rate (p-HRR), total heat release (THR), total smoke release (TSR) and total smoke production (TSP) of the two coatings. As indicated by the data in Table 3, the TTI of coating SP4 is 5 s longer than that of coating SP1, indicating that SP4 is less susceptible to ignition. The p-HRR values of coatings SP1 and SP4 are 75.46 kW/m^2 and 68.29 kW/m^2, respectively, demonstrating that coating SP4 exhibits lower flame intensity and instantaneous heat release rate during combustion. The formation of a dense carbon layer in the coating occurs at an earlier time point, which effectively retards heat transfer. Both the TSR and TSP values of coating SP4 are significantly lower than those of coating SP1, indicating that coating SP4 releases less toxic gas and particulate matter during combustion. This is attributed to the fact that CaO particles generated from the high-temperature decomposition of SE-SBIPs exhibit strong adsorption capacity for soot precursors (such as polycyclic

aromatic hydrocarbons) produced during the pyrolysis of the coating, thus inhibiting their aggregation into soot particles. Furthermore, the alkaline surface of CaO may catalyze the oxidation of soot particles and promote their conversion into CO_2, further reducing smoke production.

Table 3 Cone calorimetry test data of coatings SP1 and SP4 after water immersion

Sample	TTI/s	p-HRR/(kW/m^2)	THR/(MJ/m^2)	TSR/(m^2/m^2)	TSP/m^2
SP1	50	75.46	17.9	820.2	7.3
SP4	55	68.29	19.0	785.6	6.9

Figure 10 presents the carbon layer images (a-b) and test results c of coatings SP1 and SP4 after the cone calorimetry test. As indicated by the heat release rate (HRR) and total heat release (THR) curves of the two coatings, the peak heat release rate of coating SP4 is significantly lower than that of coating SP1, demonstrating that its flame-retardant components reduce the intensity of instantaneous combustion more effectively. This is attributed to the fact that CO_2 generated from the thermal decomposition of SE-SBIPs dilutes combustible gases, and the resulting CaO adheres to the surface of the carbon layer, further retarding heat transfer. The THR curve of coating SP4 exhibits a gentler slope, indicating that coating SP4 releases less heat per unit time and features a slower combustion rate. This confirms that the addition of SE-SBIPs delays the combustion process of the coating and effectively reduces its combustion intensity in the early stage of combustion. As reflected by the smoke production rate (SPR) and total smoke release (TSR) curves of the two coatings, both the SPR and TSR values of coating SP4 are lower than those of coating SP1 in the early combustion phase. This indicates that the addition of SE-SBIPs effectively suppresses smoke production from the coating, which is consistent with the results in Table 3.

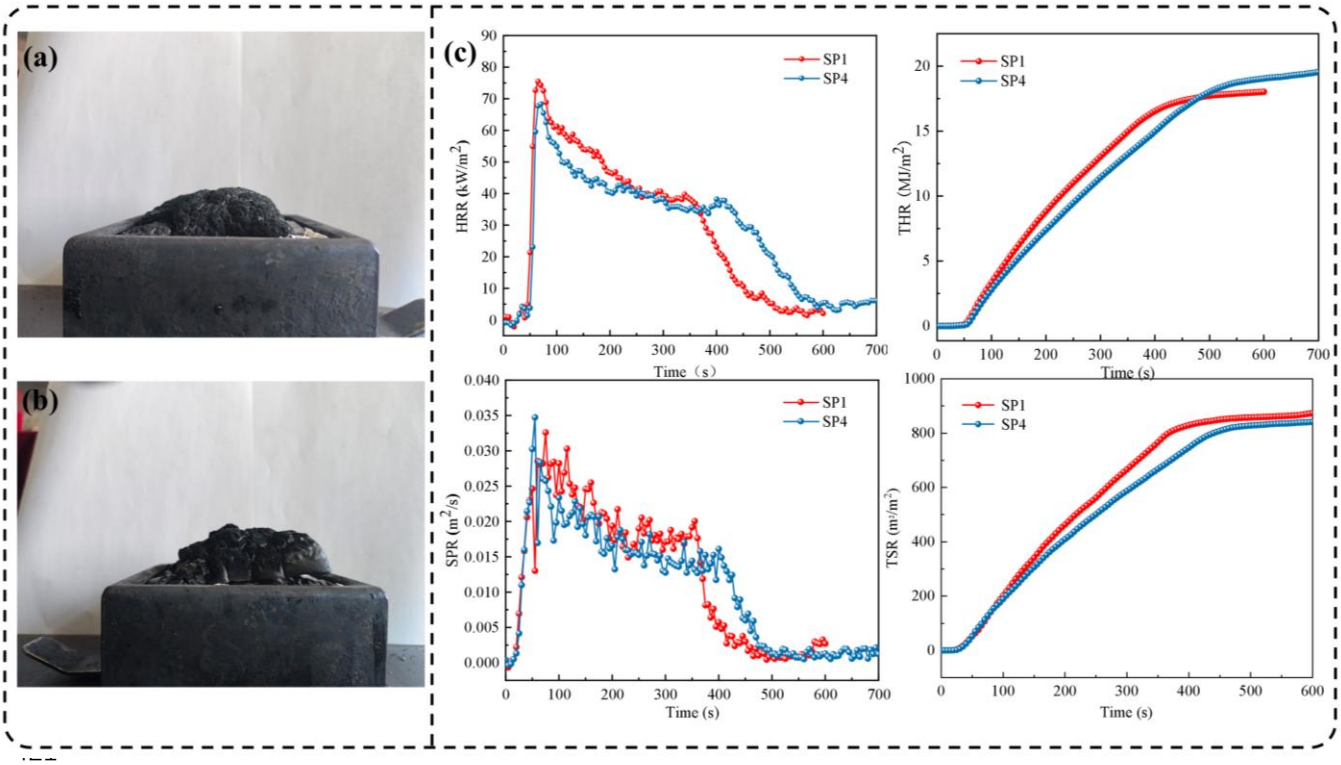


Fig.10. Carbon layer images and test results of the coating sample after the cone calorimetry test

The results demonstrate that coating SP4 doped with 3 wt.% SE-SBIPs retains good flame-retardant properties after 48 h of water immersion. It improves the fire resistance of the water-immersed coating, reduces heat release during combustion, and particularly reduces the flame intensity at the early combustion stage. In addition, it significantly reduces the total smoke release.

3.6 Analysis of Carbon Layer Strength After Water Immersion

Figures 11(a) and 11(b) present the SEM images of carbon layers of coatings SP1 and SP4 after 48 h of water immersion, obtained after the cone calorimetry test. As shown in Figure 11, expandable carbon layers with porous structures are formed on both coatings after high-temperature exposure, whereas significant differences in pore sizes and compactness are observed between the two carbon layers. The carbon layer of SP1 (without SE-SBIPs) lacks sufficient constraint during the expansion process, resulting in an irregular porous structure with relatively large pore sizes and poor overall compactness. Furthermore, distinct cracks are detected on the carbon layer due to its relatively poor flame-retardant

properties. In comparison, coating SP4 forms a denser and more continuous expanded carbon layer with a more uniform and dense pore distribution, and the pore sizes vary within a narrow range. Such a uniform pore structure is more effective in retarding heat transfer across the carbon layer. Accordingly, the incorporation of SE-SBIPs promotes the formation of a more stable thermally insulating carbon layer on the coating at high temperatures, thus reducing heat transfer between the flame and the substrate.

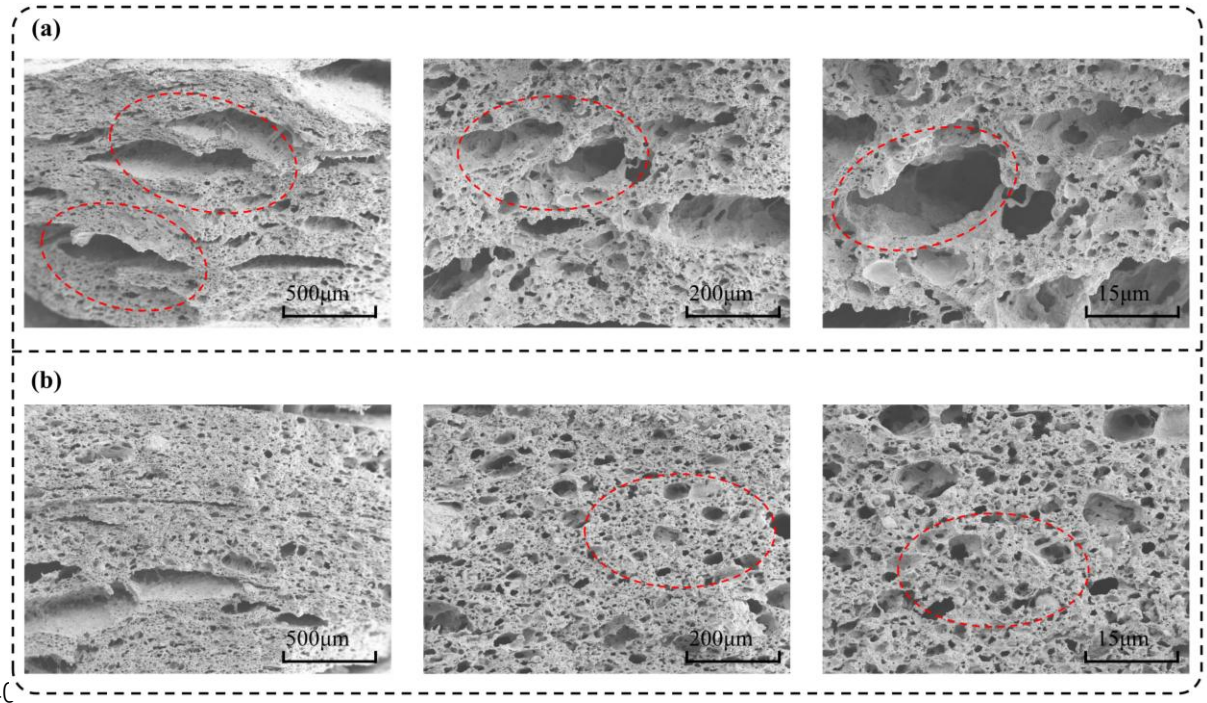


Fig.11. SEM image of the carbon layer of the coating after the cone calorimetry test

Raman spectroscopy was employed to characterize the carbon layers of coatings SP1 and SP4, with peak fitting analysis performed, and the results are shown in Figures 12(a) and 12(b). The D and G peaks of the carbon layers are detected at 1350 cm^{-1} and 1585 cm^{-1}, respectively. The G peak of the SP4 carbon layer is intense and sharp, which may indicate a higher degree of graphitization and a more ordered structure. Figure 12(a) presents the D and G peak values of the SP1 carbon layer, and the ID/IG value of the SP1 (without SE-SBIPs) is 1.36. Figure 12(b) shows the D and G peak values of the SP4 carbon layer. The results reveal that the ID/IG value of the SP4 carbon layer doped with 3 wt.% SE-SBIPs is 1.07, representing a 21.3% reduction compared with that of SP1. The SP4 carbon layer exhibits significantly

higher structural strength than the SP1 carbon layer, indicating a higher degree of graphitization, fewer structural defects and a structure closer to ideal graphite. The Raman spectroscopy results demonstrate that SE-SBIPs significantly enhances the strength of the carbon layer formed by the coating upon heating.

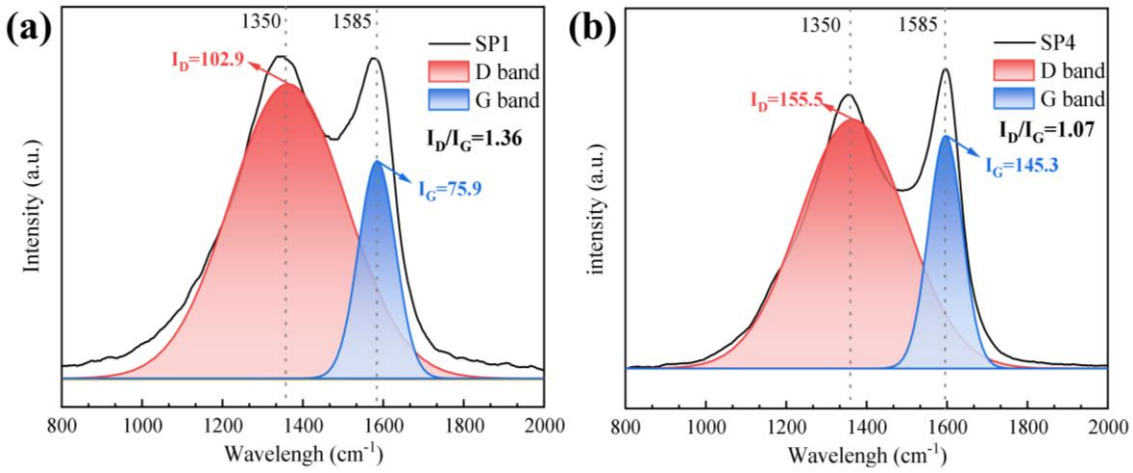


Fig.12. Raman spectral peaks of the carbon layers of SP1 (a) and SP4 (b)

SEM and Raman spectroscopy results indicate that SE-SBIPs promotes the formation of a more uniform and denser carbon layer on the coating, and significantly enhances the strength of the carbon layer. Coating SP4 doped with 3 wt.% SE-SBIPs still exhibits good fire-retardant performance after 48 h of water immersion, demonstrating that SE-SBIPs markedly improves the water resistance of the coating.

4. Conclusion

In order to further improve the comprehensive properties of intumescent flame retardant coatings (IFR-EP/SAE), SE-SBIPs were introduced in this study. The enhancement effect of the filler on the flame retardancy, water resistance and microstructure of the carbon layer of the coating was investigated. The main conclusions are as follows:

(1) The structure and thermal characterization showed that the main component of SBIPs was biocalcite with high stability, showing excellent thermal stability. After surface modification with KH-

550 silane coupling agent, the dispersion of SE-SBIPs was better, and the interfacial compatibility with resin polymer matrix was significantly enhanced.

(2) The addition of 3 wt. % SE-SBIPs showed the best synergistic flame retardant enhancement effect on the coating. At this addition amount, the peak temperature on the back of the steel plate was suppressed to 289.27℃, and the limiting oxygen index (LOI) increased to 42.5 %. At the same time, the initial rapid thermal degradation temperature of the coating jumped from 304℃ to 363℃, and the maximum mass loss rate peak shifted to the high temperature region more than 100℃, which realized the simultaneous improvement of low temperature thermal stability and final char yield.

(3) SE-SBIPs have significant advantages in improving the waterproofness of the coating and strengthening the strength of the carbon layer. After 48 hours of water immersion aging, the coating doped with 3 wt. % SE-SBIPs still maintained excellent fire resistance, and its heat release and total smoke production were greatly reduced. The formed expanded carbon layer is dense and uniform, and the structural stability is fundamentally improved.

References

1. Zhang, J, Xu, K, Reniers, G and You, G, "Statistical analysis the characteristics of extraordinarily severe coal mine accidents (ESCMAs) in China from 1950 to 2018." Process Safety and Environmental Protection, 133 332–340 (2020). https://doi.org/10.1016/j.psep.2019.10.014

2. Deng, J, Li, X, Wang, K, Wang, C, Ren, L, Qu, G and Li, Q, "Advances and prospects in risk prediction and early warning technology for the compound disaster of coal spontaneous combustion and gas explosion." Process Safety and Environmental Protection, 201 107489 (2025). https://doi.org/10.1016/j.psep.2025.107489

3. Androulakis, V, Kingman, S, Khaniani, H, Hassanalian, M, Shao, S and Roghanchi, P, "Intelligent self-evacuation path planning for fire emergencies in underground coal mines." Tunnelling and Underground Space Technology, 162 106623 (2025). https://doi.org/10.1016/j.tust.2025.106623

4. Zhang, J, Liang, Z, Liu, J, Wan, Y, Tao, X, Zhang, H and Wang, M, "Preparation and performance analysis of palygorskite reinforced silicone-acrylic emulsion-based intumescent coating." Progress in Organic Coatings, 166 106801 (2022). https://doi.org/10.1016/j.porgcoat.2022.106801

5. Lei, B, Ding, W, Zhang, Q, Lou, G, Liu, T and Dang, S, "Experimental investigation of high-temperature fire resistance properties of corrugated steel-concrete composite structures." Tunnelling and Underground Space Technology, 172 107560 (2026). https://doi.org/10.1016/j.tust.2026.107560

6. Zheng, P, Zhao, H, Li, J, Liu, Q, Ai, H, Yang, R and Xing, W, "Recent advances in constructing new type of epoxy resin flame retardant system using ammonium polyphosphate." Journal of Safety Science and Resilience, 5 (2) 179–193 (2024). https://doi.org/10.1016/j.jnlssr.2024.03.002

7. Mathews, LD, Capricho, JC, Peerzada, M, Salim, NV, Parameswaranpillai, J and Hameed, N, "Recent progress and multifunctional applications of fire-retardant epoxy resins." Materials Today

503 Communications, 33 104702 (2022). https://doi.org/10.1016/j.mtcomm.2022.104702

504 8. Price, EJ, Covello, J, Tuchler, A and Wnek, GE, "Intumescent, Epoxy-Based Flame-Retardant
505 Coatings Based on Poly(acrylic acid) Compositions." ACS APPLIED MATERIALS & INTERFACES,
506 12 (16) 18997–19005 (2020). https://doi.org/10.1021/acsami.0c00567

507 9. Cheng, C, Wang, Y, Lu, Y, Li, S, Li, H, Yan, J and Du, S, "Bio-based arginine surface-modified
508 ammonium polyphosphate: an efficient intumescent flame retardant for epoxy resin††Electronic
509 supplementary information (ESI) available. See DOI: 10.1039/d1ra09459a." RSC Advances, 12 (15)
510 9223–9237 (2022). https://doi.org/10.1039/d1ra09459a

511 10. Zhang, J, Liu, Z, Qi, P, Liu, J, Sun, J, Gu, X, Li, H, Zhao, J and Zhang, S, "Rapid-curing imidazole-
512 based highly transparent protective coating for polycarbonate films with good hardness and flame
513 retardancy." Progress in Organic Coatings, 189 108289 (2024).
514 https://doi.org/10.1016/j.porgcoat.2024.108289

515 11. Zhan, W, Gu, Z, Jiang, J and Chen, L, "Influences of surface area of graphene on fire protection of
516 waterborne intumescent fire resistive coating." Process Safety and Environmental Protection, 139 106–
517 113 (2020). https://doi.org/10.1016/j.psep.2020.04.004

518 12. Li, G, Yang, J, He, T, Wu, Y and Liang, G, "An Investigation of the thermal degradation of the
519 intumescent coating containing MoO3 and Fe2O3." Surface and Coatings Technology, 202 (13) 3121–
520 3128 (2008). https://doi.org/10.1016/j.surfcoat.2007.11.016

521 13. Hu, X, Zhu, X and Sun, Z, "Effect of $CaAlCO_3$-LDHs on fire resistant properties of intumescent
522 fireproof coatings for steel structure." Applied Surface Science, 457 164–169 (2018).
523 https://doi.org/10.1016/j.apsusc.2018.06.165

524 14. Pappalardo, S, Russo, P, Acierno, D, Rabe, S and Schartel, B, "The synergistic effect of organically

525 modified sepiolite in intumescent flame retardant polypropylene." European Polymer Journal, 76 196–
526 207 (2016). https://doi.org/10.1016/j.eurpolymj.2016.01.041
527 15. Xie, W, Chen, H, He, D, Zhang, Y, Fu, L, Ouyang, J and Yang, H, "An emerging mineral-based
528 composite flame retardant coating: Preparation and enhanced fireproof performance." Surface and
529 Coatings Technology, 367 118–126 (2019). https://doi.org/10.1016/j.surfcoat.2019.03.073
530 16. Fan, F-q, Xia, Z-b, Li, Q-y and Li, Z, "Effects of inorganic fillers on the shear viscosity and fire
531 retardant performance of waterborne intumescent coatings." Progress in Organic Coatings, 76 (5) 844–
532 851 (2013). https://doi.org/10.1016/j.porgcoat.2013.02.002
533 17. Zhan, W, Chen, L, Cui, F, Gu, Z and Jiang, J, "Effects of carbon materials on fire protection and
534 smoke suppression of waterborne intumescent coating." Progress in Organic Coatings, 140 105491
535 (2020). https://doi.org/10.1016/j.porgcoat.2019.105491
536 18. Chen, C, Xiao, G, Dong, S, Zhong, F, Yang, Z, Chen, C, Wang, M and Zou, R, "Construction of
537 CMS@MoS_2 core-shell structure to enhance flame retardancy and smoke suppression performance of
538 waterborne epoxy fireproof coatings for steel structures." Colloids and Surfaces A: Physicochemical and
539 Engineering Aspects, 633 127836 (2022). https://doi.org/10.1016/j.colsurfa.2021.127836
540 19. Sun, Y, Yuan, B, Shang, S, Zhang, H, Shi, Y, Yu, B, Qi, C, Dong, H, Chen, X and Yang, X, "Surface
541 modification of ammonium polyphosphate by supramolecular assembly for enhancing fire safety
542 properties of polypropylene." Composites Part B: Engineering, 181 107588 (2020).
543 https://doi.org/10.1016/j.compositesb.2019.107588
544 20. Lim, KS, Bee, ST, Sin, LT, Tee, TT, Ratnam, CT, Hui, D and Rahmat, AR, "A review of
545 application of ammonium polyphosphate as intumescent flame retardant in thermoplastic compos
546 ites." COMPOSITES PART B-ENGINEERING, 84 155–174 (2016). https://doi.org/10.1016/j.com

positesb.2015.08.066

21. Xu, Z, Liu, D, Yan, L and Xie, X, "Synergistic effect of sepiolite and polyphosphate ester on the fire protection and smoke suppression properties of an amino transparent fire-retardant coating." Progress in Organic Coatings, 141 105572 (2020). https://doi.org/10.1016/j.porgcoat.2020.105572

22. Chaisaenrith, P, Taksakulvith, P and Pavasupree, S, "Effect of nano titanium dioxide in intumescent fireproof coating on thermal performance and char morphology." Materials Today: Proceedings, 47 3462–3467 (2021). https://doi.org/10.1016/j.matpr.2021.03.461

23. Zhang, W, Xiang, Y, Jiang, W, Yang, Z, Zhang, L and Li, B, "Preparation of MUF/α-ZrP@MnHP@APP composite nanolayered flame retardant coating for application on expanded polystyrene (EPS) foam." Chemical Engineering Journal, 524 169600 (2025). https://doi.org/10.1016/j.cej.2025.169600

24. Shi, Y and Wang, G, "An intumescent flame retardant containing caged bicyclic phosphate and oligomer: Synthesis, thermal properties and application in intumescent fire resistant coating." Progress in Organic Coatings, 90 83–90 (2016). https://doi.org/10.1016/j.porgcoat.2015.10.003

25. Zhan, W, Ni, L, Gu, Z, Cui, F, Jiang, J and Chen, L, "The influences of graphene and carbon nanotubes on properties of waterborne intumescent fire resistive coating." Powder Technology, 385 572–579 (2021). https://doi.org/10.1016/j.powtec.2021.03.018

26. Yan, L, Xu, Z and Wang, X, "Influence of nano-silica on the flame retardancy and smoke suppression properties of transparent intumescent fire-retardant coatings." Progress in Organic Coatings, 112 319–329 (2017). https://doi.org/10.1016/j.porgcoat.2017.07.017

27. Fu, A, Ulusoy, B, Ahmadi, H, Wu, H and Dam-Johansen, K, "Intumescent coatings: Comprehensive advances with a focus on inorganic-dominant systems." Progress in Organic Coatings, 199 108939

(2025). https://doi.org/10.1016/j.porgcoat.2024.108939

28. Zhang, Y, Sun, Y, Du, W, Dong, H, Wang, B, Wang, Y and Cao, X, "Preparation and characteristic study of the hydrogel of coal spontaneous combustion environmental protection." Fuel, 360 130505 (2024). https://doi.org/10.1016/j.fuel.2023.130505

29. Tu, Z, Ou, H, Ran, Y, Xue, H and Zhu, F, "Chitosan-based biopolyelectrolyte complexes intercalated montmorillonite: A strategy for green flame retardant and mechanical reinforcement of polypropylene composites." International Journal of Biological Macromolecules, 277 134316 (2024). https://doi.org/10.1016/j.ijbiomac.2024.134316

30. Liu, L, He, H, Feng, X, Yu, B, Yang, H and Tawiah, B, "Bio-based supramolecular intumescent coatings for wood fire protection." Polymer Degradation and Stability, 247 111965 (2026). https://doi.org/10.1016/j.polymdegradstab.2026.111965

31. Wang, F, Liu, H and Yan, L, "Comparative Study of Fire Resistance and Char Formation of Intumescent Fire-Retardant Coatings Reinforced with Three Types of Shell Bio-Fillers." Polymers (Basel), 13 (24) (2021). https://doi.org/10.3390/polym13244333

32. Tuble, KAQ, Omisol, CJM, Abilay, GY, Tomon, TRB, Aguinid, BJM, Dumancas, GG, Malaluan, RM and Lubguban, AA, "Synergistic effect of phytic acid and eggshell bio-fillers on the dual-phase fire-retardancy of intumescent coatings applied on cellulosic substrates." Chemosphere, 358 142226 (2024). https://doi.org/10.1016/j.chemosphere.2024.142226

33. Roopan, SM, "An overview of natural renewable bio-polymer lignin towards nano and biotechnological applications." International Journal of Biological Macromolecules, 103 508–514 (2017). https://doi.org/10.1016/j.ijbiomac.2017.05.103

34. Yew, MC, Ramli Sulong, NH, Yew, MK, Amalina, MA and Johan, MR, "Eggshells: A novel bio-filler

591 for intumescent flame-retardant coatings." Progress in Organic Coatings, 81 116–124 (2015).
592 https://doi.org/10.1016/j.porgcoat.2015.01.003
593 35. Beh, JH, Yew, MK, Yew, MC and Saw, LH, "Characterization and fire protection properties of
594 rubberwood biomass ash formulated intumescent coatings for steel." Journal of Materials Research and
595 Technology, 14 2096–2106 (2021). https://doi.org/10.1016/j.jmrt.2021.07.103
596 36. Nasir, KM, Sulong, NHR, Johan, MR and Afifi, AM, "Synergistic effect of industrial- and bio-fillers
597 waterborne intumescent hybrid coatings on flame retardancy, physical and mechanical properties."
598 Progress in Organic Coatings, 149 105905 (2020). https://doi.org/10.1016/j.porgcoat.2020.105905
599 37. Ren, J, Piao, J, Wang, Y, Wang, Y, Feng, T, Liu, W, Dong, H, Chen, W, Jiao, C and Che
600 n, X, "Effect of functionalized oyster shell powder with ammonium polyphosphate on fire safet
601 y performance of epoxy resin." Progress in Organic Coatings, 172 107054 (2022). https://doi.or
602 g/10.1016/j.porgcoat.2022.107054
603 38. Du, W, Wang, Y, Wang, L, Cao, X and Zhu, G, "Preparation and performance analysis of an
604 intumescent fire-retardant coating with strong water resistance." Applied Surface Science, 706 163596
605 (2025). https://doi.org/10.1016/j.apsusc.2025.163596